Available online at www.sciencedirect.com
SCIENCE DIRECT®
ELSEVIER
Journal of Magnetism and Magnetic Materials 260 (2003) 78–83
journal of magnetism and magnetic materials
www.elsevier.com/locate/jmmm

The oxidation state at tunnel junction interfaces

Xavier Batlle[a,*], Bart Jan Hattink[a], Amílcar Labarta[a], Johan J. Åkerman[b], Roberto Escudero[b,1], Ivan K. Schuller[b]

[a] *Dept. Física Fonamental, Facultat de Física, Universitat Barcelona, Av. Diagonal 647, 08028-Barcelona, Catalonia, Spain*
[b] *Physics Department-0319, University of California — San Diego, La Jolla, CA 92093-0319, USA*

Received 29 January 2002; received in revised form 23 July 2002

Abstract

The oxidation state at the interfaces of Nb/Al–AlO_x/Pb junctions is discussed. Conductance–voltage curves below and above the superconducting temperature suggest tunneling conduction, while X-ray photoelectron spectroscopy shows the existence of a thin AlO_x layer at the Nb/Al interface. We demonstrate that at the usual 10^{-7} Torr range of base pressures in the sputtering chamber, this is due to the time elapsed between the deposition of the Nb and Al bottom layers, in both Nb/Al–AlO_x/Pb tunnel junctions and Nb/Al bilayers. We also give some direct evidence of the oxidation of the top Pb electrode on the Nb electrode surface. Such oxidation probably occurs at the pinholes of the intermediate Al–AlO_x layer of the tunnel junctions, as a consequence of the oxidation state at the Nb/Al interface, which helps to avoid barrier shorts and enhances the quality of the tunnel barrier. We therefore suggest that there is oxide formation in other places besides where there is an actual oxide deposited. This is relevant for the performance of magnetic tunnel junctions since in most tunneling studies it is assumed that once the oxide is deposited, that is the only place where there is an oxide. This is also a very general statement applicable to thin film systems.

Keywords: Tunnel junctions; Oxidation at interfaces; X-ray photoelectron spectroscopy

1. Introduction

Ferromagnet/insulator/ferrromagnet (FM/I/FM) magnetic tunnel junctions (MTJs) exhibiting large magnetoresistance (MR) [1] have lately attracted much interest due to their potential applications [2,3]. The performance of the junctions is strongly dependent on the oxidation of the FM electrodes at the FM/I interfaces, as well as on the oxidation state of the barrier, which has to be homogenous and complete. The use of thinner and thinner barriers has reopened the question of how to rule out the presence of pinholes. Rowell and others developed a set of criteria to ascertain that tunneling is the dominant mechanism in junctions with at least one superconducting (S) electrode [4]. Three of these criteria still apply in FM/I/FM structures: (i) an exponential insulator thickness dependence of the conductance, G; (ii) a parabolic voltage dependence of G that can be fitted to the

*Corresponding author. Tel.: +34-93-402-1155; fax: +34-93-402-1149.
E-mail address: xavier@ffn.ub.es (X. Batlle).
[1] Permanent address: IIM-UNAM, Mexico City, D.F., Apartado Postal 70-360, Mexico.

0304-8853/03/$ - see front matter
PII: S0304-8853(02)01177-0

theoretical models [5,6]; and (iii) a weak insulating-like temperature dependence $G(T)$.

For the first criterion, it has been shown [7] that pinholes may mimic the exponential thickness dependence of the tunneling resistance. For the second one, some of us demonstrated [8] that S/I/FM junctions that displayed parabolic $G(V)$ curves in the normal state, showed, at low temperatures and depending on the oxidation procedure, either tunneling or pinhole conduction (Andreev reflection [9]). The recent observation of very large MR in Co–Co and Ni–Ni wire nanocontacts [10] also suggests the pinhole contribution to TMR in MTJs. Given the ratio of the conduction between metallic contacts and junctions [11], pinhole regions of one part in 10^6 must be ruled out to ensure no pinhole conduction in parallel with tunneling. For the third criterion, some results suggest that pinholes yield a metallic-like temperature dependence of the junction resistance [8,12]. Therefore, out of the three Rowell criteria, only one, the insulating-like $G(T)$, seems to be reliable. Recently, some of us have proposed a new set of quality criteria for the identification of barrier shorts in MTJs [13].

X-ray photoelectron spectroscopy (XPS) [14] is an excellent technique for the analysis of MTJs [15] since it is sensitive to the chemical species as well as to their bonding state. In this paper, the oxidation state at the interfaces of Nb/Al–AlO_x/Pb junctions is discussed. Conductance–voltage curves below and above the superconducting temperature suggest tunneling conduction, while X-ray photoelectron spectroscopy indicates that, at the usual 10^{-7} Torr range of base pressures in the sputtering chamber, there exists a thin oxygen layer mostly adsorbed on the surface of the bottom electrode that yields the oxidation of the first impinging atoms of the intermediate layer. We also demonstrate that this is due to the time elapsed between the deposition of the layers. These observations evidence oxide formation at other places than the intended oxide layer. Therefore, the oxidation state at the interfaces may strongly affect the tunneling process by modifying the pinhole conductivity and the interface chemistry and roughness.

2. Experimental

The junctions were prepared as follows [8]: a DC sputtered superconducting Nb(80 nm)/Al(10 nm) bilayer bottom electrode was oxidized in air for 10 min and a Pb top electrode (200 nm) was deposited in a separate thermal evaporation unit, leading to the Nb/Al–AlO_x/Pb junction (Pb sample). Nb was chosen as the base electrode since the superconducting temperature T_c is high ($T_c = 9.22$ K for the bulk material; good films display T_c values within the range 8–9 K [16]). The resulting Al oxide thickness was typically 1–2 nm and the remaining 8 nm of metallic Al were superconducting ($T_c = 8$–9 K) for proximity to the Nb [16]. For a second sample, the bottom electrode was oxidized for 18 h in air (barrier thickness of 2–3 nm) and a Ni (20 nm) layer was DC sputtered on top, leading to the Nb/Al–AlO_x/Ni junction (Ni sample). The junction area for both samples was $1 \times 0.3\,\mathrm{mm}^2$. These two samples are representative of the variety of samples studied [8]. Standard AC (1 kHz) differential conductance $G = \mathrm{d}I/\mathrm{d}V$ measurements as a function of DC bias were carried out from 4.2 to 300 K using a balanced bridge. XPS spectra (Al K_α; base pressure 10^{-9} Torr) were recorded for exactly the same samples as in $G(V)$. The distribution of elements across the junction was studied by performing a low-energy sputtering process (4 keV, incident at 45°; typical etching rate 6–10 nm/min) for a short time (6–18 s) and recording the spectrum after each step. This sputtering process, which may lead to a certain intermixing, together with the fact that the XPS signal averages the out-coming electrons from a region of about 5–10 nm in depth, precludes the observation of sharp interfaces.

3. Results and discussion

For the Pb junction, $G(V)$ at 155 K suggests tunnel conduction (Fig. 1(a)), which is confirmed by the signature of the superconducting gap at 4.2 K (inset of Fig. 1(a)): reduced conductance at $V = 0$, two symmetric maxima just outside the gap at $\pm\Delta = 1.3$ meV, and phonon features outside the gap. $G(V)$ at 4.2 K has been fitted to a

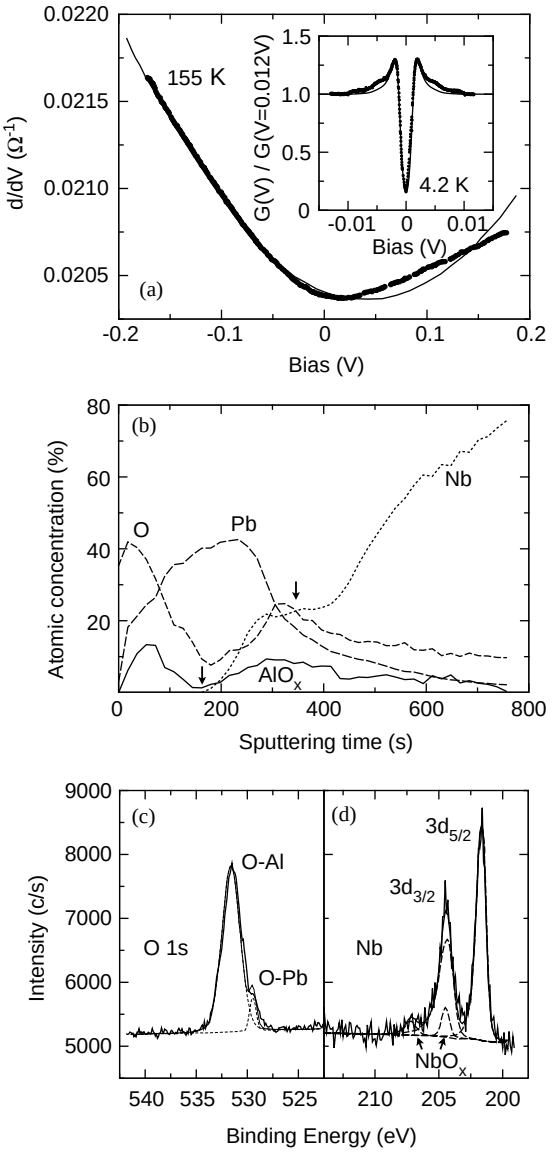

Fig. 1. Nb/Al–AlO_x/Pb junction: (a) $G(V)$ curve at 155 K, together with a fit to the BDR model [5]. Inset. $G(V)$ curve at 4.2 K, showing the superconducting gap (tunnel conduction). The solid line represents the fitting of the data to a thermally smeared BCS tunneling curve [17]. (b) Atomic concentration obtained from the XPS intensities for Pb, O, AlO_x and Nb, as a function of the sputtering time. (c) Example of the XPS spectra for the O 1s core level at the Nb/Al interface (sputtering time: 324 s), showing the O–Al and O–Pb (3%) contributions. (d) Nd 3d core level (sputtering time: 216 s), showing the NbO contribution.

thermally smeared Bardeen–Cooper–Schrieffer (BCS) tunneling curve (inset of Fig. 1(a)). The good agreement proves that single-step electron tunneling dominates the transport, without any significant leakage current [17]. From the fit we extract $\Delta_{Nb/Al} + \Delta_{Pb} = 1.3$ meV at 4.2 K. The literature value of $\Delta_{Pb}(4.2\,K) = 0.9$ meV suggests that the gap of the Al at the oxide interface is about 0.4 meV, due to the proximity effect with the Nb. The fit of $G(V)$ at 155 K to the Brinkman–Dynes–Rowell (BDR) model [5] yields a barrier thickness of 1.1 nm and heights of 3.6 and 2.4 eV on the Pb and Nb/Al sides, respectively, while the fit to the Simmons' model [6] yields 1.2 nm and 2.9 eV. For the Ni sample, G is high and flat, indicating big metal-to-metal shorts. This suggests that Pb mostly adds to the AlO_x barrier without damaging it and that the latter is free of metal-to-metal pinholes. On the contrary, Ni damages the barrier, which might be due to the fact that the Ni top electrode was deposited by sputtering, while the Pb electrode was deposited by evaporation. The difference between sputtering and evaporation is that for the former the energy distribution of atoms arriving at the substrate surface depends very sensitively on the target–substrate distance and the sputtering pressure. It was shown, based on numerical calculations [18], that this can be more or less disruptive depending on the particular experimental configuration and therefore no universal conclusion can be obtained. The influence of the top electrode material on the junction properties might also be considered: both the junction resistance [19] and the barrier height [20] increase with the ionic radius (from Ni to Pb) since the larger the latter is, the less the element can penetrate into the barrier, resulting in less effective micro-shorts.

Fig. 1(b) shows the atomic concentration of Nb, Pb, AlO_x and O obtained from the XPS intensities [14] for the Pb sample, as a function of the sputtering time (sputtering steps of 18 s). The AlO_x concentration was obtained by fitting the intensity of the Al 2p core level to both a metallic and oxide contribution [14]. As soon as Nb is detected, the O signal increases, first reaching a maximum and later decreasing as the sputtering process approaches the Nb layer. The AlO_x concentration

perfectly follows that of O (Fig. 1(b)), the first maximum corresponding to the insulating barrier, the second one (ca. 300 s) suggesting that there is a thin oxygen layer on top of Nb that oxidizes the first Al atoms arriving at the bottom electrode. At short sputtering times, the oxidation of both the free surface of the sample (O–Pb 1s at 528.3–529.4 eV) and the barrier (O–Al 1s at 531–531.5 eV) are observed. Besides, the O–Al 1s peaks at the Nb/Al interface are clearly asymmetric at low energies, and a small peak at about 529.3 eV is observed (Fig. 1(c)), suggesting an O–Pb contribution of about 3%. This indicates that some PbO_x is present on the Nb surface, which is probably due both to the existence of the oxygen layer at the Nb/Al interface and to the consequent Pb oxidation at the pinholes of the Al–AlO_x layer. This is in agreement with some electron microscopy studies showing a pinhole surface area up to about 2% in AlO_x barriers [21], even if in the present Pb junction, the former Al layer was about 10 nm in thickness. In addition, some redistribution of oxygen between the different layers may also occur. From the Nb 3d core level (Fig. 1(d)), some NbO (Nb–O $3d_{5/2}$ at 204.6 eV) on the surface of the Nb layer is inferred, although the calculated O–Nb contribution is at least one order of magnitude smaller than the experimental O–Al one, so that the former (530.0–530.4 eV) is not detected since it overlaps the latter. The Pb 4f core level (not shown) at the Nb/Al interface also yields a small amount of PbO and/or Pb_3O_4, while the O–Pb/Pb–O ratio is about 1.5. The effective barrier height extracted from the BDR or Simmons models (Fig. 1(a)) may thus reflect a contribution from the oxidation state at the Nb/Al interface, either from AlO_x and PbO_x (pinholes) or/and from NbO_x. The Ni sample also follows this framework: both the O–Al 1s and Al–O 2p signals increase on the surface of Nb. However, we note that, as the barrier is disrupted, the direct relation of the milling time to absolute depth for the Ni structure should be taken as tentative.

Given the base pressures in the sputtering chamber (2.6×10^{-7} and 1.3×10^{-7} Torr for the Pb and Ni samples, respectively), the thin oxygen layer at the Nb/Al interface is related to the time that the Nb film is kept in the chamber before the Al deposition proceeds (45 min and 5 h for the Pb and Ni junctions, respectively). Three Nb(100 nm)/Al(20 nm) bilayers were prepared to support this suggestion: sample Nb/Al-1, for which the Nb layer was 100 s in chamber (base pressure of 1.4×10^{-7} Torr); sample Nb/Al-2, for which the Nb layer was 18.5 h in the chamber (1.2×10^{-7} Torr); and sample Nb/Al-3, for which the Nb layer was 27 h in air (former base pressure of 1.4×10^{-7} Torr). The role of the standard Gibbs energy of formation of the metal oxides ($\Delta_f G_0$ at 298.15 K) [22] was studied by preparing two Nb(100 nm)/Pb(200 nm) bilayers with increasing transfer time in air from the sputtering chamber to the Pb evaporation unit; sample Nb/Pb-1 was 7 min in air, while sample Nb/Pb-2, was 24 h.

The atomic concentration for Nb, metallic Al, O and AlO_x for the Nb/Al bilayers is shown in Fig. 2 as a function of the sputtering time (sputtering step of 6 s). The AlO_x concentration at the Nb/Al interface clearly increases with increasing time between the Nb and Al depositions. Even for sample Nb/Al-1 (Fig. 2(a)), there is a change in the slope of both the concentrations of AlO_x and O as the Nb layer is detected. The O 1s core level yields mostly O–Al bonds and, although there might be some NbO on the surface of the Nb, the calculated O–Nb contribution is at least about one order of magnitude smaller than the O–Al one for all samples, in agreement with $\Delta_f G_0(Al_2O_3) = -1582.3$ kJ/mol and $\Delta_f G_0(NbO) = -378.6$ kJ/mol [22]. XPS results do not reflect a progressive oxidation of the Al target during the time elapsed between the deposition of the Nb and Al layers, since (i) both the Al and Nb targets were pre-sputtered before the deposition of Nb, and (ii) while Nb is being sputtered (and during the time delay), the Al gun is turned on. We note that Al wets Nb much better than it wets a transition metal FM. As the thin oxygen layer absorbed on top of Nb affects the initial growth of the Al layer, this effect is thus expected to be enhanced in MTJs. A similar picture is drawn for the Nb/Pb samples (not shown), the main differences being that, while at the free surface of the samples the oxidation state corresponds to O–Pb, in agreement with the Pb–O contribution to the Pb 4f core level,

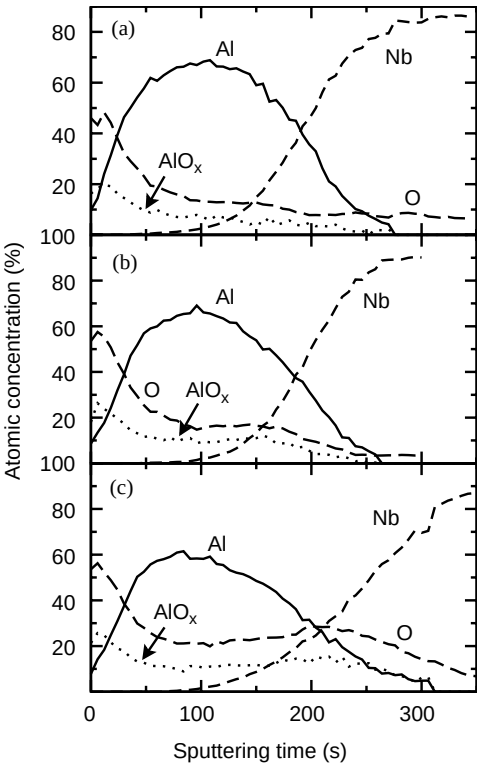

Fig. 2. (a) Atomic concentration obtained from the XPS intensities for Al, O, AlO_x and Nb, as a function of the sputtering time, for sample Nb/Al-1 (Nb layer kept 100 s in the sputtering chamber; base pressure of 1.4×10^{-7} Torr). (b) Same data for sample Nb/Al-2 (18.5 h, 1.2×10^{-7} Torr). (c) Same data for sample Nb/Al-3 (27 h in air).

the O 1s increase at the Nb/Pb interface takes place at 530.0–530.4 eV, suggesting that this is the core level energy for the O–Nb 1s bonds. Both the Nb-O peak position and the O–Nb/Nb–O ratio at the Nb/Pb interfaces, suggest NbO_2. Besides, the calculated O–Pb contribution is about two orders of magnitude smaller than the O–Nb one, in agreement with $\Delta_f G_0(NbO_2) = -740.5\,kJ/mol$ and $\Delta_f G_0(PbO) = -187.9\,kJ/mol$ [22]. $\Delta_f G_0$ is also much larger (in absolute value) for the Al oxides than that for the typical Fe and Co oxides [22]. Consequently, the oxidation state at the bottom FM/I interface in MTJs will also be dependent on the synthesis conditions.

In conclusion, we have shown that in Nb/Al–AlO_x/Pb junctions with dominant tunnel conduction and prepared at the usual 10^{-7} Torr base pressures, the oxidation state at the interfaces depends on the time elapsed between the deposition of the layers. We have also given some direct evidence of the oxidation of the top electrode on the surface of the bottom one, probably at the pinholes of the intermediate layer—even if the latter is about 10 nm in thickness—and due to the oxidation state at the interfaces and redistribution of oxygen between different layers. It is thus suggested that all the foregoing helps to avoid barrier shorts and enhances the quality of the tunnel barrier. The true tunneling barrier seems to be a combination of the various oxides both from the expected barrier itself as from the oxidation state at the bottom Nb/Al interface. The existence of pinholes in the Al film is not so surprising: The actual effective Al thickness for pinholes is only of a few nanometers [21], taking into account the uncertainty in the nominal Al thickness (10–15%), the thickness of the AlO_x barrier grown by natural oxidation in air (probably displaying pinholes [8]), the oxygen layer adsorbed on top of the Nb surface, and the surface roughness of the Nb layer. We note that other authors [23] have already suggested that in junctions with sputtered oxide barriers and Pb top electrodes, the relevant tunneling barrier is the natural oxide grown on suface of the bottom electrode due to pinholes in the sputtered oxide. These results show oxide formation in other places besides where there is an actual oxide deposited. This is relevant since most tunneling studies do not take this possibility into account, which is also a very general statement applicable to thin film systems. Consequently, the oxidation state at the interfaces may be relevant to the dominant conduction mechanism in MTJs, the relative metal oxide formation energy of the selected elements being crucial.

Acknowledgements

Financial support of the Spanish CICYT (MAT2000-0858) and the Generalitat de Catalunya (ACI2000-04 and 2000SGR-025) are gratefully recognized. I.K.S. acknowledges US DARPA and DOE. X.B. is indebted to Dr. J.L. Alay

(Scientific and technical facilities, University of Barcelona) for technical support during XPS experiments.

References

[1] J.S. Moodera, L.R. Kinder, T.M. Wong, R. Meservey, Phys. Rev. Lett. 74 (1995) 3273;
T. Miyazaki, N. Tezuka, J. Magn. Magn. Mater. 139 (1995) L231.
[2] J.M. Daughton, J. Appl. Phys. 81 (1997) 3758.
[3] W.J. Gallagher, S.S.P. Parkin, Y. Lu, X.P. Bian, A. Marley, K.P. Roche, R.A. Altman, S.A. Rishton, C. Jahnes, T.M. Shaw, J. Appl. Phys. 81 (1997) 3741.
[4] E. Burnstein, S. Lundqvist (Eds.), Tunneling Phenomena in Solids, Plenum, New York, 1969.
[5] W.F. Brinkman, R.C. Dynes, J.M. Rowell, J. Appl. Phys. 41 (1970) 1915.
[6] J.G. Simmons, J. Appl. Phys. 34 (1963) 1793.
[7] D.A. Rabson, J.J. Åkerman, A.H. Romero, R. Escudero, C. Leigthon, S. Kim, I.K. Schuller, J. Appl. Phys. 89 (2001) 2786.
[8] J.J. Åkerman, R. Escudero, C. Leigthon, S. Kim, I.K. Schuller, Appl. Phys. Lett. 77 (2000) 1870.
[9] G.E. Blonder, M. Tinkham, T.M. Klapwijk, Phys. Rev. B 25 (1982) 4515.
[10] G. Tatara, Y.W. Zhao, M. Muñoz, N. García, Phys. Rev. Lett. 83 (1999) 2030 and references therein.
[11] W.P. Pratt Jr., S.-F. Lee, J.M. Slaughter, R. Loloee, P.A. Schoeder, J. Bass, Phys. Rev. Lett. 66 (1991) 3060.
[12] U. Rüdiger, R. Calarco, U. May, K. Samm, H. Kittur, G. Güntherodt, J. Appl. Phys. 89 (2001) 7573.
[13] J.J. Åkerman, J.M. Slaughter, R.W. Dave, I.K. Schuller, Appl. Phys. Lett. 79 (2001) 3104.
[14] D. Briggs, M.P. Seah (Eds.), Practical Surface Analysis, John Wiley, New York, 1983;
J. Chastain (Ed.), Handbook of X-ray Photoelectron Spectroscopy, Perkin-Elmer Corporation, Eden Prairie, 1992.
[15] S.R. Qiu, H.F. Lai, J.A. Yarmoff, Phys. Rev. Lett. 85 (2000) 1492;
P. LeClair, J.T. Kohlhepp, A.A. Smits, H.J.M. Swagten, B. Koopmans, W.J.M. de Jonge, J. Appl. Phys. 87 (2000) 6070;
H.A.M. de Gronckel, H. Kohlstedt, C. Daniels, Appl. Phys. A 70 (2000) 435;
J. Kwo, G.K. Wertheim, M. Gurvitch, D.N.E. Buchanan, Appl. Phys. Lett. 40 (1982) 675;
Z. Zhang, S. Cardoso, P.P. Freitas, X. Batlle, P. Wei, N. Barradas, J.C. Soares, J. Appl. Phys. 89 (2001) 6665;
J. Wang, P.P. Freitas, E. Snoeck, X. Batlle, J. Cuadra, J. Appl. Phys. 91 (2002) 7463;
X. Batlle, B.J. Hattink, A. Labarta, J.J. Åkerman, R. Escudero, I.K. Schuller, J. Appl. Phys. 91 (2002) 10163.
[16] A. Zehnder, Ph. Lerch, S.P. Zhao, Th. Nussbaumer, E.C. Kirk, H.R. Ott, Phys. Rev. B 59 (1999) 8875.
[17] I. Giaever, H.R. Hart Jr., K. Mergele, Phys. Rev. 126 (1962) 941.
[18] K.E. Meyer, I.K. Schuller, C.M. Falco, J. Appl. Phys. 52 (1981) 5803.
[19] R.M. Handy, Phys. Rev. 126 (1962) 1968.
[20] Y.B. Ning, M.C. Gallagher, J.G. Adler, Phys. Rev. B 37 (1988) 6139.
[21] D. Ozkaya, R.E. Dunin-Borkowski, A.K. Petford-Long, P.K. Wong, M.G. Blamire, J. Appl. Phys. 87 (2000) 5200.
[22] D.R. Lide (Ed.), CRC Handbook of Chemistry and Physics, 78th Edition, CRC Press, Boca Raton, FL., 1997.
[23] C.L. Platt, A.S. Katz, R.C. Dynes, A.E. Berkowitz, Appl. Phys. Lett. 75 (1999) 127.